

Scenario analysis with multivariate Bayesian machine learning models

Michael PFARRHOFER
WU Vienna

Anna STELZER
Oesterreichische Nationalbank

We present an econometric framework that adapts tools for scenario analysis, such as conditional forecasts and generalized impulse response functions, for use with dynamic nonparametric multivariate models. We demonstrate the utility of this approach through an exercise with simulated data, and three real-world applications: (i) scenario-based conditional forecasts aligned with Federal Reserve Bank stress test assumptions, (ii) measuring macroeconomic risk under varying financial conditions, and (iii) the asymmetric effects of US-based financial shocks and their international spillovers. Our results indicate the importance of nonlinearities and asymmetries in the dynamic relationship between macroeconomic and financial variables.

JEL: C11, C32, C53, C54

Keywords: conditional forecast, generalized impulse response function, Bayesian additive regression trees, nonlinearities, (semi)-structural inference

Contact: Michael Pfarrhofer (michael.pfarrhofer@wu.ac.at), Department of Economics, WU Vienna University of Economics and Business. We would like to thank Niko Hauzenberger for useful comments.

Disclaimer: The views expressed in this paper do not necessarily reflect those of the Oesterreichische Nationalbank or the Eurosystem.

1. INTRODUCTION

In this paper, we discuss how to conduct scenario analysis with multivariate time series models in a macroeconomic context when the functional form of the conditional mean is nonlinear and/or unknown. This situation can arise when relying on “traditional” nonlinear frameworks (e.g., in variants of threshold, regime-switching, or time-varying parameter models, see Fischer *et al.* (2023) for a recent example), but is virtually always the case in recently developed models that introduce Bayesian machine learning (ML) techniques to multivariate macroeconometric modeling (see, e.g., Huber and Rossini, 2022; Clark *et al.*, 2023; Huber *et al.*, 2023; Hauzenberger *et al.*, 2024c).

We use the term scenario analysis broadly to refer to different types of counterfactual experiments, including a version of conditional forecasts and variants of generalized impulse response functions (GIRFs, see Koop *et al.*, 1996). While some aspects and issues in this context have been discussed in isolation in the aforementioned papers, there is no unified explicit treatment or comprehensive framework available yet. Inspired by the closely related work of Crump *et al.* (2025), which focuses on a linear Bayesian vector autoregression (VAR), this is the gap in the literature that we aim to fill with our paper.

Conditional forecasts — the simulation of the future path of selected variables conditional on predefined scenarios encoded in constraints placed on observed variables — have been used by academics and practitioners since the 1980s in a *linear* VAR context (see, e.g., Doan *et al.*, 1984), with subsequent refinements and improvements in computational efficiency (see, e.g., Waggoner and Zha, 1999; Jarociński, 2010; Bańbura *et al.*, 2015). A recent and highly efficient computational approach is developed in Chan *et al.* (2025). Their framework exploits the properties of conditionally Gaussian errors in conjunction with the common assumption of a known linear conditional mean relationship. The full future path of restricted and unrestricted forecasts across multiple horizons can be jointly sampled from a high-dimensional (potentially truncated) multivariate Gaussian distribution.

Breaking the assumption of linearity complicates matters. In particular, the presence

of nonlinearities makes it difficult to derive multi-step ahead predictive distributions, and in many cases it will be outright impossible to obtain closed-form solutions. In this case, one can resort to recursive predictive simulation. This paper discusses how common approaches to conditional forecasting can be adapted to the context of nonparametric multivariate models. The proposed approach is quite general in the sense that it can be used in conjunction with most popular frameworks that introduce nonlinearities in the conditional mean of multivariate models. The key assumption is that the reduced form errors are conditionally multivariate Gaussian.

Since the impulse response function (IRF), another key macroeconomic estimand, is commonly defined as the difference between forecasts conditioned on the values of different shocks, our proposed framework is also useful for semi-structural scenario analysis in a nonlinear context (see [Antolin-Diaz *et al.*, 2021](#), for an excellent discussion when using linear structural VARs, SVARs). Specifically, we revisit the issue of how to obtain dynamic causal effects, in the form of GIRFs, in a nonlinear and possibly nonparametric context. We examine both unrestricted GIRFs to shocks identified with approaches typically used in the linear SVAR literature, and restricted GIRFs, which can be used to investigate and quantify the contributions of specific sets of transmission channels in the propagation of structural shocks. The latter are obtained by partially matching the moments of the unconditional and conditional predictive distributions used to compute the GIRFs.

We mentioned above that the proposed approach is quite generally applicable in multivariate models whenever one is willing to assume conditionally Gaussian innovations. This means that there is a large number of potential candidates for the respective conditional mean functions that can be assumed. These choices include (but are not limited to) regression tree-based implementations, Gaussian process priors, or neural networks (see [Marcellino and Pfarrhofer, 2024](#), for a recent Bayesian overview). For our empirical work, we use Bayesian Additive Regression Trees (BART, [Chipman *et al.*, 2010](#)) as a specific nonparametric implementation to infer functional relationships in a multivariate time series model. We pick this sum-of-trees model because tree-based approaches have proven particularly capable of producing accurate forecasts when used with time series

data for the US economy (see, e.g., Medeiros *et al.*, 2021; Goulet Coulombe *et al.*, 2022; Clark *et al.*, 2023; Goulet Coulombe, 2024), with datasets typically structured similarly to the one we use in this paper.

Our approach to scenario analysis is developed under the assumption of a multivariate Gaussian error term with a general time-varying covariance matrix. From a practical and implementation perspective, we rely on a somewhat simplified version to capture time variation of the respective volatilities. The framework allows for flexible equation-by-equation estimation of the multivariate system and offers significant improvements in computational efficiency also in the context of conditional forecasts and GIRFs. In our empirical work, we capture heteroskedastic features of the data with a specification related to common volatility approaches (see Carriero *et al.*, 2016), which also reflects recent tools used to address outliers during the Covid-19 pandemic (see, e.g., Carriero *et al.*, 2024). It is worth noting that all methods also work with more sophisticated volatility models (see, e.g., Chan, 2023), albeit at the cost of increased computational burden.

After investigating the performance our approach with synthetic data, we apply our framework in several related yet distinct cases. Our dataset comprises about 25 quarterly macroeconomic and financial variables for the US economy ranging from the mid-1970s to the last quarter of 2023. In one of our explorations, we also add some international variables and include data from the euro area (EA), Japan, and the United Kingdom (UK) in our model. The applied work assesses and illustrates the role of nonlinearities when interest centers on conditional forecasts, and we also explore asymmetries in the propagation of structural shocks of different signs and magnitudes. Specifically, we provide three empirical applications. First, inspired by Chan *et al.* (2025), we use a subset of the assumptions underlying the annual stress test conducted by the Federal Reserve System and compute conditional forecasts using soft constraints for different scenarios, comparing predictive densities from linear and nonlinear models. Second, reflecting the growth-at-risk literature (see Adrian *et al.*, 2019), we study the counterfactual implications of varying financial conditions (imposing hard constraints over a period) on tail risks of output growth, inflation, and employment. Third, we identify a US-based financial shock

(as in, e.g., Barnichon *et al.*, 2022), and compute GIRFs to shocks of different signs and magnitudes that are allowed to propagate internationally. We then use a restricted GIRF approach to gauge the role of spillovers and spillbacks.

The rest of this paper is structured as follows. Section 2 lays out the baseline econometric framework and discusses an implementation using BART. Section 3 provides remarks about obtaining predictive inference with Monte Carlo methods. We discuss how to impose hard and soft constraints on forecasts, and how these constraints may be used to construct semi-structural scenarios through generalized impulse response functions. Section 4 provides an empirical illustration of the proposed methods. The last section concludes.

2. ECONOMETRIC FRAMEWORK

Let $\mathbf{y}_t = (y_{1t}, \dots, y_{nt})'$ collect n variables for $t = 1, \dots, T$, and $\mathbf{x}_t = (\mathbf{y}'_{t-1}, \dots, \mathbf{y}'_{t-p})'$ is a $k \times 1$ vector that stacks lags of \mathbf{y}_t , thus $k = np$. We use a multivariate model of the form:

$$\mathbf{y}_t = \mathbf{F}(\mathbf{x}_t) + \boldsymbol{\epsilon}_t, \quad \boldsymbol{\epsilon}_t \sim \mathcal{N}(\mathbf{0}_n, \boldsymbol{\Sigma}_t), \quad (1)$$

where $\mathbf{F}(\mathbf{x}_t) = (f_1(\mathbf{x}_t), \dots, f_n(\mathbf{x}_t))'$ is an n -vector of conditional mean functions $f_i(\mathbf{x}_t) : \mathbb{R}^k \rightarrow \mathbb{R}$ for $i = 1, \dots, n$, such that $\mathbf{F}(\mathbf{x}_t) : \mathbb{R}^k \rightarrow \mathbb{R}^n$. One may assume a specific functional form for the $f_i(\mathbf{x}_t)$'s or treat them as unknown and estimate them. The methods we discuss in this paper are designed specifically for the latter case. We assume zero mean Gaussian errors $\boldsymbol{\epsilon}_t$ with $n \times n$ time-varying covariance matrix $\boldsymbol{\Sigma}_t$.

2.1. Multivariate system estimation

To estimate the multivariate (reduced form) model in Equation (1) efficiently from a computational perspective, we rely on a conditional representation of its n equations. Let \mathbf{e}_i of size $1 \times n$ denote the i th row of an identity matrix \mathbf{I}_n , and \mathbf{E}_i of size $(n-1) \times n$

is the matrix resulting from deleting the i th row of \mathbf{I}_n . Using $\mathbf{y}_{-it} = \mathbf{E}_i \mathbf{y}_t$ we may write $\mathbf{y}_t = \mathbf{e}'_i y_{it} + \mathbf{E}'_i \mathbf{y}_{-it}$. Under the assumptions of Equation (1) one may derive the conditional distribution:¹

$$p(y_{it} | \mathbf{y}_{-it}, \bullet) \propto \exp \left\{ -\frac{1}{2} (\mathbf{e}_i \boldsymbol{\Sigma}_t^{-1} \mathbf{e}'_i y_{it}^2 - 2y_{it} \mathbf{e}_i \boldsymbol{\Sigma}_t^{-1} (\mathbf{F}(\mathbf{x}_t) - \mathbf{E}'_i \mathbf{y}_{-it})) \right\},$$

which is a Gaussian with variance $\varsigma_{it}^2 = (\mathbf{e}_i \boldsymbol{\Sigma}_t^{-1} \mathbf{e}'_i)^{-1}$ and mean $\mu_{it} = \varsigma_{it}^2 (\mathbf{e}_i \boldsymbol{\Sigma}_t^{-1} (\mathbf{F}(\mathbf{x}_t) - \mathbf{E}'_i \mathbf{y}_{-it}))$. Indeed, this distribution is equivalent to a more common representation of the conditional multivariate Gaussian (see, e.g., Cong *et al.*, 2017, Section 2, Equation 5). The mean can alternatively be written as $\mu_{it} = f_i(\mathbf{x}_t) + \varsigma_{it}^2 (\mathbf{e}_i \boldsymbol{\Sigma}_t^{-1} \mathbf{E}'_i) (\mathbf{y}_{-it} - \mathbf{E}_i \mathbf{F}(\mathbf{x}_t))$, and we define $\tilde{\mu}_{it} = \varsigma_{it}^2 (\mathbf{e}_i \boldsymbol{\Sigma}_t^{-1} \mathbf{E}'_i) (\mathbf{y}_{-it} - \mathbf{E}_i \mathbf{F}(\mathbf{x}_t))$, i.e., $\mu_{it} = f_i(\mathbf{x}_t) + \tilde{\mu}_{it}$.

The i th equation of the multivariate model in regression form, conditional on all other equations, is then given by:

$$(y_{it} - \tilde{\mu}_{it}) = f_i(\mathbf{x}_t) + u_{it}, \quad u_{it} \sim \mathcal{N}(0, \varsigma_{it}^2), \quad (2)$$

which can be used in a Gibbs sampler to update the conditional mean relationships by looping through equations $i = 1, \dots, n$. This approach is similar to the one of Esser *et al.* (2024) and allows to treat each equation of the multivariate system individually, conditional on all other equations.

¹Earlier related contributions often either use a mapping between the structural and reduced form of the VAR to enable equation-by-equation estimation (see, e.g., Hauzenberger *et al.*, 2024c), or rely on factor models for the reduced form errors (see, e.g., Clark *et al.*, 2023). These approaches come with computational and inferential advantages and disadvantages. The former is simple to implement but requires parameterizing the structural form which may cause associated issues such as breaking order-invariance of the equations. The latter allows for order-invariant inference but gives rise to the usual identification challenges of factor models. Our proposed approach allows for directly working with the reduced form model, and obtaining order-invariant inference.

2.2. Bayesian Additive Regression Trees

The approach we discuss in Section 3 works with any implementation of multivariate models with jointly Gaussian errors. That is, assuming a linear functional form for $\mathbf{F}(\mathbf{x}_t)$ results in a standard BVAR.² In case we choose to treat $\mathbf{F}(\mathbf{x}_t)$ nonparametrically, several options are available. Due to its versatility and the established favorable empirical properties we mentioned earlier, we use BART to approximate the equation-specific functions in our applied work. That is, we consider a sum of $s = 1, \dots, S$, tree functions $\ell_{is}(\mathbf{x}_t | \mathcal{T}_{is}, \mathbf{m}_{is})$:

$$f_i(\mathbf{x}_t) \approx \sum_{s=1}^S \ell_{is}(\mathbf{x}_t | \mathcal{T}_{is}, \mathbf{m}_{is}),$$

where \mathcal{T}_{is} are regression trees and \mathbf{m}_{is} is a vector of terminal node parameters (which serve as fitted values). Instead of having a single but complex tree, BART is akin to ensemble methods, and uses a sum of many simple trees (“weak learners”), which has been shown to work well empirically.

Using BART requires an algorithm that estimates splitting variables and thresholds for which we specify suitable priors that together yield $p(\mathcal{T}_{is})$; we further need a prior on the terminal node parameters $p(\mathbf{m}_{is} | \mathcal{T}_{is})$. Our setup follows Chipman *et al.* (2010) and we first define the probability that a tree ends at a specific node at depth $d = 0, 1, 2, \dots$, as $\alpha / (1 + d)^\beta$, with $\alpha \in (0, 1)$ and $\beta \in \mathbb{R}^+$. This prevents trees from getting overly complex and provides regularization (here, we rely on the default values $\alpha = 0.95$, and $\beta = 2$, which perform well across many datasets). For the splitting variables, we choose a uniform prior. This implies that each predictor is equally likely to be selected as a splitting variable. We further assign a uniform prior to all thresholds within the splitting rules, based on the range of the respective splitting variable.

²When we consider linear versions of our model for comparisons, we implement this setting with $\mathbf{F}(\mathbf{x}_t) = \mathbf{A}\mathbf{x}_t$ where \mathbf{A} is an $n \times k$ matrix of reduced form VAR coefficients. We assume a horseshoe prior with a single global shrinkage parameter on these coefficients, see also Hauzenberger *et al.* (2024b). Equation (2) can be used to update the VAR coefficients equation-by-equation from their usual Gaussian posteriors.

Next we specify the prior for the terminal node parameters. On these parameters $\mathbf{m}_{i_s,l}$, for $l = 1, \dots, \#\text{TN}_{i_s}$, where $\#\text{TN}_{i_s}$ denotes the number of terminal node parameters of tree s in equation i , we impose independent conjugate Gaussian priors that are symmetric across trees and identical for all terminal nodes. As suggested by Chipman *et al.* (2010) the moments of these priors are chosen in a data-driven manner, such that 95% of the prior probability lies in the interval $(\min(\mathbf{y}_i), \max(\mathbf{y}_i))$, where $\mathbf{y}_i = (y_{i1}, \dots, y_{iT})'$, and such that shrinkage increases the more trees S are chosen for estimation. We choose $S = 250$ trees which has been shown to work well for typical macroeconomic time series applications (see, e.g., Huber *et al.*, 2023).

2.3. Priors on other model parameters

The methods discussed in this paper work with a general time-varying covariance matrix Σ_t . Significant computational advantages, however, are available if one assumes that $\Sigma_t = s_t \Sigma$, i.e., that the covariance structure only varies proportionally over time. The prior setup for the constant part of the covariance matrix follows Esser *et al.* (2024). Specifically, we use a hierarchical inverse Wishart prior:

$$\Sigma | \{a_i\}_{i=1}^n \sim \mathcal{W}^{-1}(s_0, \mathbf{S}_0),$$

where $s_0 = \nu + n - 1$, $\mathbf{S}_0 = 2\nu \cdot \text{diag}(1/a_1, \dots, 1/a_n)$ and $a_i \sim \mathcal{G}^{-1}(1/2, 1/A_j^2)$ for $i = 1, \dots, n$, and a fixed scale parameter $A_j > 0$; see also Huang and Wand (2013). Setting $\nu = 2$ implies a comparatively uninformative prior about the implied correlation structure, different from fixed-hyperparameter versions of this prior.

In case we model time-varying variances, we follow Carriero *et al.* (2024) and assume that:

$$s_t^{1/2} = \begin{cases} 1 & \text{with probability } 1 - \mathbf{p} \\ \mathcal{U}(2, \bar{\mathbf{s}}) & \text{with probability } \mathbf{p}, \end{cases}$$

where $\mathcal{U}(2, \bar{s})$ is a discrete uniform distribution with (integer) support between 2 and $\bar{s} = 6$ and $\mathbf{p} \sim \mathcal{B}(a_p, b_p)$ is the probability associated with observing an outlier. Alternative models related to common stochastic volatility specifications are available in this context. More flexible approaches, such as those discussed in Chan (2020, 2023), are straightforward to implement, but may significantly increase the computational burden.

2.4. Posterior distributions and sampling algorithm

We may use the conditional distribution in Equation (2) to update the trees equation-by-equation using the backfitting approach designed by Chipman *et al.* (2010); see also Esser *et al.* (2024). Here, one may define the vector of partial residuals

$$\tilde{y}_{is,t} = \left(y_{it} - \tilde{\mu}_{it} - \sum_{j \neq s} \ell_{ij}(\mathbf{x}_t | \mathcal{T}_{ij}, \mathbf{m}_{ij}) \right) \sim \mathcal{N}(\ell_{is}(\mathbf{x}_t | \mathcal{T}_{is}, \mathbf{m}_{is}), \zeta_{it}^2),$$

conditioning on the fit of each of the $S - 1$ trees except tree s and information in all but the i th equation. In full data notation, $\tilde{\mathbf{y}}_{is} = (\tilde{y}_{is,1}, \dots, \tilde{y}_{is,T})'$, this defines a conditionally Gaussian likelihood, $p(\tilde{\mathbf{y}}_{is} | \mathcal{T}_{is}, \mathbf{m}_{is}, \bullet)$, which can be marginalized analytically over the terminal node parameters \mathbf{m}_{is} (to keep the dimensionality of the inferential problem fixed).

Combining this conditional likelihood with the prior on the trees, and a suitable transition density (based on four distinct moves: grow a terminal node, prune a terminal node, change a splitting rule, swap a child/parent node), the trees are sampled using a standard accept/reject Metropolis-Hastings algorithm. These trees (and associated rules) partition the input space and we obtain a distinct set of observations for each terminal node. The posterior then takes the conventional Gaussian form for these parameters.

Updating all trees $s = 1, \dots, S$, across equations $i = 1, \dots, n$, yields an updated fit that can be used to compute the outlier-adjusted residuals $\boldsymbol{\epsilon}_t / \sqrt{s_t} = \mathbf{y}_t - \mathbf{F}(\mathbf{x}_t)$. The posterior of the constant part of the covariance matrix is then given by:

$$\boldsymbol{\Sigma} | \bullet \sim \mathcal{W}^{-1} \left(s_0 + T, \mathbf{S}_0 + \sum_{t=1}^T s_t^{-1} \boldsymbol{\epsilon}_t \boldsymbol{\epsilon}_t' \right)$$

The hierarchical parameters of the prior on the covariance matrix can be updated using:

$$a_i | \bullet \sim \mathcal{G}^{-1} \left(\frac{\nu + T}{2}, \frac{1}{A_i^2} + \nu \cdot \Sigma_{[ii]}^{-1} \right),$$

where $\Sigma_{[ii]}^{-1}$ denotes the i th diagonal element of Σ^{-1} . The outlier adjustment parameter s_t can be sampled, due to its discrete support, using the probabilities:

$$\Pr(s_t^{1/2} = 1 | \mathbf{y}_t, \mathbf{F}(\mathbf{x}_t), \Sigma, \mathbf{p}) \propto \mathcal{N}(\mathbf{y}_t | \mathbf{F}(\mathbf{x}_t), \Sigma) \cdot (1 - \mathbf{p}),$$

$$\Pr(s_t^{1/2} = \mathfrak{s} | \mathbf{y}_t, \mathbf{F}(\mathbf{x}_t), \Sigma, \mathbf{p}) \propto \mathcal{N}(\mathbf{y}_t | \mathbf{F}(\mathbf{x}_t), \mathfrak{s}\Sigma) \cdot (\mathbf{p}/(\bar{\mathfrak{s}} - 1)), \quad \text{for } \mathfrak{s} = 2, 3, \dots, \bar{\mathfrak{s}},$$

on a t -by- t basis. The posterior distribution of the outlier probability is $\mathbf{p} | \bullet \sim \mathcal{B}(a_{\mathbf{p}} + T_o, b_{\mathbf{p}} + T - T_o)$, with the total number of observations classified as outliers denoted by $T_o = \sum_{t=1}^T \mathbb{I}(s_t \neq 1)$, where $\mathbb{I}(\bullet)$ is an indicator function that yields 1 if its argument is true and 0 otherwise.

This completes our modeling framework and algorithmic implementation. We turn to the issue of predictive and structural inference next.

3. PREDICTIVE SIMULATION

Define a vector Ξ that contains all coefficients and latent variables necessary to parameterize Equation (1). At time τ , the one-step-ahead predictive distribution is given by the integral:

$$p(\mathbf{y}_{\tau+1} | \mathcal{I}) = \int p(\mathbf{y}_{\tau+1} | \mathcal{I}, \Xi) p(\Xi | \mathcal{I}) d\Xi, \quad (3)$$

where \mathcal{I} denotes the respective information set used to infer Ξ . For out-of-sample forecasts, \mathcal{I} is typically given by $\{\mathbf{y}_t\}_{t=1}^{\tau}$, and we are interested in predicting $\mathbf{y}_{\tau+h} | \{\mathbf{y}_t\}_{t=1}^{\tau}$ for $h = 1, 2, \dots$, steps ahead. In other cases we may also want to condition on the full information set, i.e., \mathcal{I} is given by $\{\mathbf{y}_t\}_{t=1}^T$, to compute hypothetical scenarios in-sample for $\tau \in \{1, 2, \dots, T\}$ using the distribution of $\mathbf{y}_{\tau+h} | \{\mathbf{y}_t\}_{t=1}^T$ conditional on parameters

informed by the full information set. In either case, the distribution $p(\mathbf{y}_{\tau+1} | \mathcal{I})$ in general does not take a well-known form, and neither does the distribution of higher-order forecasts for $h \geq 2$.

However, we may still explore and obtain random samples from them via predictive simulation. This involves exploiting the fact that even though $p(\mathbf{y}_{\tau+1} | \mathcal{I})$ is unknown, $p(\mathbf{y}_{\tau+1} | \mathcal{I}, \Xi)$ takes a conditionally Gaussian form under the quite flexible model of Equation (1). Let m denote the current iteration of the MCMC algorithm and $x^{(m)}$ indicates the m th draw of a random variable. The one-step-ahead predictive distribution is given by:

$$p(\mathbf{y}_{\tau+1} | \mathcal{I}, \Xi^{(m)}) = \mathcal{N}(\mathbf{F}^{(m)}(\mathbf{x}_{\tau+1}), \Sigma_{\tau+1}^{(m)}), \quad (4)$$

where $\mathbf{x}_{\tau+1} = (\mathbf{y}'_{\tau}, \dots, \mathbf{y}'_{\tau-p+1})'$. For $h \geq 2$ we may iterate forward, conditioning recursively on the draws for preceding horizons, by setting the predictors to $\mathbf{x}_{\tau+h}^{(m)} = (\mathbf{y}_{\tau+h-1}^{(m)'} , \mathbf{y}_{\tau+h-2}^{(m)'} , \dots)'$, and obtain:

$$p(\mathbf{y}_{\tau+h} | \mathcal{I}, \mathbf{y}_{\tau+1:\tau+h-1}^{(m)}, \Xi^{(m)}) = \mathcal{N}(\mathbf{F}^{(m)}(\mathbf{x}_{\tau+h}^{(m)}), \Sigma_{\tau+h}^{(m)}), \quad (5)$$

where $\mathbf{y}_{\tau+1:\tau+h-1}^{(m)}$ denotes the path of the variables from $\tau+1$ to $\tau+h-1$ and $\mathbf{y}_{\tau+1:\tau+h} = (\mathbf{y}'_{\tau+1}, \dots, \mathbf{y}'_{\tau+h})'$. This exploits the fact that:

$$p(\mathbf{y}_{\tau+1:\tau+h} | \mathcal{I}) = \int p(\mathbf{y}_{\tau+1} | \mathcal{I}, \Xi) \prod_{j=2}^h p(\mathbf{y}_{\tau+j} | \mathbf{y}_{\tau+1}, \dots, \mathbf{y}_{\tau+j-1}, \mathcal{I}, \Xi) p(\Xi | \mathcal{I}) d\Xi, \quad (6)$$

that is, the joint distribution of forecasts can be decomposed into the product of the conditional one-step ahead predictive densities. Simulating the process forward, by sampling from the distribution in Equation (5) across horizons $h = 1, 2, \dots$, in each sweep of our algorithm, delivers draws from $p(\mathbf{y}_{\tau+1:\tau+h} | \mathcal{I})$, via Monte Carlo integration.

3.1. Conditional forecasts

Suppose we want to impose restrictions on a predefined path of one or more variables. Formally, this implies an additional conditioning argument for the predictive distribution, see also Crump *et al.* (2025) for related discussions. In this context, we denote by \mathcal{C}_h a set that defines the desired restrictions at horizon $h = 1, 2, \dots$, i.e., the unconditional forecast results when $\mathcal{C}_h = \emptyset$ for all h , and $\mathcal{C}_{1:h} = \{\mathcal{C}_1, \dots, \mathcal{C}_h\}$. In our version, interest centers on the conditional distribution $p(\mathbf{y}_{\tau+1:\tau+h} | \mathcal{I}, \mathcal{C}_{1:h})$, which in line with Equation (6) can be written as:

$$p(\mathbf{y}_{\tau+1:\tau+h} | \mathcal{I}, \mathcal{C}_{1:h}) = \int p(\mathbf{y}_{\tau+1:\tau+h} | \mathcal{I}, \mathcal{C}_{1:h}, \Xi) p(\Xi | \mathcal{I}) d\Xi,$$

$$p(\mathbf{y}_{\tau+1:\tau+h} | \mathcal{I}, \mathcal{C}_{1:h}, \Xi) = p(\mathbf{y}_{\tau+1} | \mathcal{I}, \mathcal{C}_1, \Xi) \prod_{j=2}^h p(\mathbf{y}_{\tau+j} | \mathbf{y}_{\tau+1}, \dots, \mathbf{y}_{\tau+j-1}, \mathcal{I}, \mathcal{C}_{1:j}, \Xi).$$

That is, we again decompose the joint distribution across horizons as a product of the sequence of conditional one-step ahead distributions. We thus impose the restrictions h -by- h recursively at each point in time and jointly simulate the restricted and unrestricted variables forward for each iteration of our sampling algorithm.

Notably this differs from the “traditional” implementation of conditional forecasts, that impose the conditions as $p(\mathbf{y}_{t+j} | \mathcal{C}_{1:h}, \bullet)$ instead of $p(\mathbf{y}_{t+j} | \mathcal{C}_{1:j}, \bullet)$ for $j = 1, \dots, h$. Put simply, our approach “filters” forward in a loose sense of the word by conditioning on the history of restrictions, thereby resulting in a future path of the unrestricted variables that is consistent with the imposed restrictions over the full set of horizons. By contrast, versions in the spirit of Waggoner and Zha (1999) condition on future restrictions as well as past (and current) ones at each horizon, either by drawing the entire paths of the reduced form shocks or by smoothing via backwards recursions (see Bańbura *et al.*, 2015, for an excellent discussion).

In static multivariate problems these two approaches coincide, while, intuitively, they will potentially lead to increasingly different results as the persistence of the underlying dynamic processes increases. We explore this apparent limitation and the practical

usefulness of our approach below in an exercise using artificial data. For dynamic systems featuring a small to moderate amount of persistence (e.g., as in typical applications with monthly/quarterly macroeconomic and financial data that are transformed towards approximate stationarity), the two versions' outputs are usually close.

Constraints. We operationalize two distinct versions of the restrictions. Define the selection matrix \mathbf{R}_h of size $r_h \times n$, where r_h is the number of restrictions which may vary across horizons. This matrix serves to select the respective restricted variables. There are two main cases of importance: *hard* and *soft* constraints. In the former case, some variables exactly follow a predetermined path; in the latter, they lie within a predetermined interval. As this interval narrows, the soft-constrained case approaches the hard-constrained one. We store these restrictions in the vector \mathbf{r}_h of size $r_h \times 1$, whereas $\underline{\mathbf{r}}_h$ and $\overline{\mathbf{r}}_h$, both of size $r_h \times 1$, denote the lower and upper bounds of an interval. For hard constraints, we have an equality restriction (see Equation 7), while the soft constraints require an inequality restriction (see Equation 8):

$$\mathcal{C}_h = \{\mathbf{R}_h \mathbf{y}_{\tau+h} = \mathbf{r}_h\}, \quad (7)$$

$$\mathcal{C}_h = \{\underline{\mathbf{r}}_h \leq \mathbf{R}_h \mathbf{y}_{\tau+h} \leq \overline{\mathbf{r}}_h\}. \quad (8)$$

To simplify notation, we omit the m -superscript that labels MCMC draws in what follows, but stress that the following computations are carried out in each sweep of our sampling algorithm, thereby marginalizing over the parameters. In addition, define the matrix \mathbf{U}_h of dimension $(n - r_h) \times n$, which mirrors the selection matrix \mathbf{R}_h and is used to select all unrestricted variables. Define the restricted, $\mathbf{y}_{\tau+h}^{(R)} = \mathbf{R}_h \mathbf{y}_{\tau+h}$, and unrestricted, $\mathbf{y}_{\tau+h}^{(U)} = \mathbf{U}_h \mathbf{y}_{\tau+h}$, subvectors of $\mathbf{y}_{\tau+h}$. Similar to the derivation in Section 2.1 and as in Chan *et al.* (2023), using Equation (5), we may then write:

$$\begin{aligned} \mathbf{y}_{\tau+h} &= \mathbf{R}'_h \mathbf{y}_{\tau+h}^{(R)} + \mathbf{U}'_h \mathbf{y}_{\tau+h}^{(U)}, \\ \mathbf{R}'_h \mathbf{y}_{\tau+h}^{(R)} + \mathbf{U}'_h \mathbf{y}_{\tau+h}^{(U)} &\sim \mathcal{N}(\mathbf{F}(\mathbf{x}_{\tau+h}), \Sigma_{\tau+h}). \end{aligned}$$

This representation can be used to obtain the conditional distribution $p(\mathbf{y}_{\tau+h}^{(U)} | \mathbf{y}_{\tau+h}^{(R)} = \mathbf{r}_h, \bullet)$, which is proportional to:

$$\exp \left\{ -\frac{1}{2} (\mathbf{y}_{\tau+h}^{(U)})' \mathbf{U}_h \boldsymbol{\Sigma}_{\tau+h}^{-1} \mathbf{U}_h' \mathbf{y}_{\tau+h}^{(U)} - 2 \mathbf{y}_{\tau+h}^{(U)}' \mathbf{U}_h \boldsymbol{\Sigma}_{\tau+h}^{-1} (\mathbf{F}(\mathbf{x}_{\tau+h}) - \mathbf{R}_h' \mathbf{y}_{\tau+h}^{(R)}) \right\}.$$

This is the kernel of a Gaussian distribution, so under the hard restriction in Equation (7), we obtain:

$$\mathbf{y}_{\tau+h}^{(U)} | \mathbf{y}_{\tau+h}^{(R)} = \mathbf{r}_h, \bullet \sim \mathcal{N}(\mathbf{m}_{\tau+h}^{(U)}, \mathbf{S}_{\tau+h}^{(U)}), \quad (9)$$

with moments $\mathbf{S}_{\tau+h}^{(U)} = (\mathbf{U}_h \boldsymbol{\Sigma}_{\tau+h}^{-1} \mathbf{U}_h')^{-1}$ and $\mathbf{m}_{\tau+h}^{(U)} = \mathbf{S}_{\tau+h}^{(U)} (\mathbf{U}_h \boldsymbol{\Sigma}_{\tau+h}^{-1} (\mathbf{F}(\mathbf{x}_{\tau+h}) - \mathbf{R}_h' \mathbf{y}_{\tau+h}^{(R)}))$.

The inequality restrictions of Equation (8) imply that the conditional forecast of interest, $p(\mathbf{y}_{\tau+h} | \underline{\mathbf{r}}_h \leq \mathbf{y}_{\tau+h}^{(R)} \leq \overline{\mathbf{r}}_h, \bullet)$, follows a truncated multivariate Gaussian distribution. Since typically only a subset of variables is restricted (i.e., $r_h \leq n$), Chan *et al.* (2025) suggest a blocked updating scheme to unlock computational advantages. Note that one may decompose the joint distribution of the restricted and unrestricted variables into two parts, and first sample from the r_h -dimensional (rather than n -dimensional) truncated multivariate Gaussian:

$$\mathbf{y}_{\tau+h}^{(R)} | \underline{\mathbf{r}}_h \leq \mathbf{y}_{\tau+h}^{(R)} \leq \overline{\mathbf{r}}_h, \bullet \sim \mathcal{N}(\mathbf{m}_{\tau+h}^{(R)}, \mathbf{S}_{\tau+h}^{(R)}) \cdot \mathbb{I}(\underline{\mathbf{r}}_h \leq \mathbf{y}_{\tau+h}^{(R)} \leq \overline{\mathbf{r}}_h),$$

with moments $\mathbf{S}_{\tau+h}^{(R)} = \mathbf{R}_h \boldsymbol{\Sigma}_{\tau+h} \mathbf{R}_h'$ and $\mathbf{m}_{\tau+h}^{(R)} = \mathbf{R}_h \mathbf{F}(\mathbf{x}_{\tau+h})$. An iid draw from this distribution, $\mathbf{y}_{\tau+h}^{(R,m)}$, can be obtained from this distribution using the minimax tilting method of Botev (2017). One may then set $\mathbf{r}_h = \mathbf{y}_{\tau+h}^{(R,m)}$, and use Equation (9) to draw the unconstrained forecasts.

Simulation. To assess the performance and implications of our recursive approach relative to alternative “traditional” implementations of conditional forecasts, we provide a comparison with the precision sampler proposed in Chan *et al.* (2025). Assuming the conditional mean function to be linear allows to contrast both algorithms one-to-one (we cannot use the precision sampler for nonlinear implementations). For this purpose, we

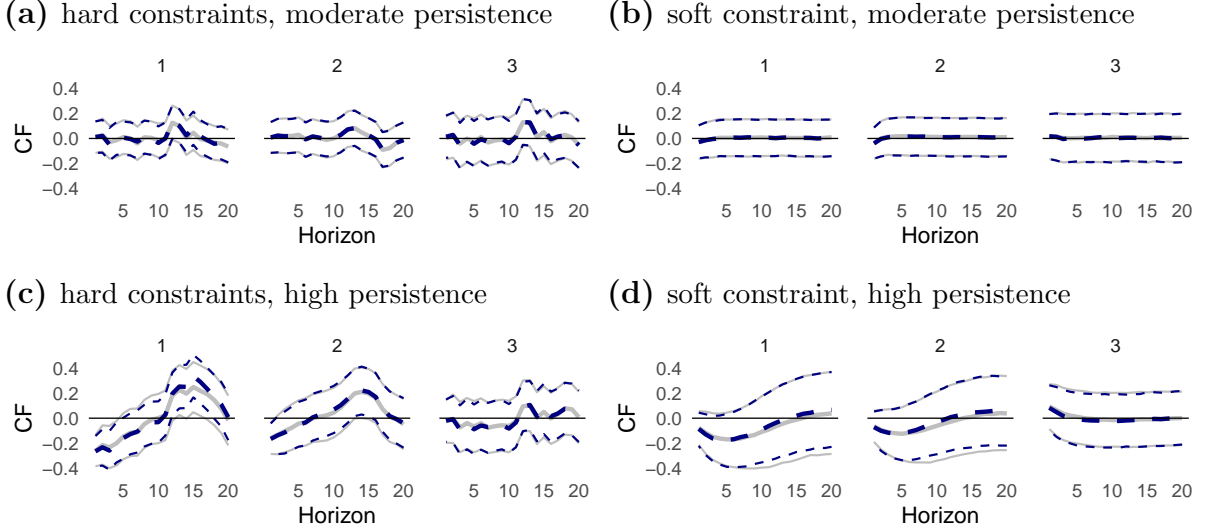


Figure 1: Conditional forecast (CF) under *moderate* and *high* levels of persistence of the underlying data generating process (DGP).

Notes: Variables 1, 2, 3. Lines refer to the percentiles 16/50/84 of the predictive distributions (*solid grey*: recursive simulation; *dashed navy blue*: precision sampling). The DGP is a VAR with $n = 6$ variables and $p = 4$ lags. The scenario *hard constraints* conditions on the realizations of three variables and leaves the others unrestricted; *soft constraint* restricts one of the variables to a predefined interval.

simulate artificial data from a linear VAR process with $n = 6$, $p = 4$ and a maximum horizon $h = 20$ for different levels of persistence (which we measure through spectral radius $\rho(\tilde{\mathbf{A}})$, i.e., the maximum absolute eigenvalues of the companion matrix of the VAR, $\tilde{\mathbf{A}}$). We label $\rho(\tilde{\mathbf{A}}) \approx 0.6$ as *moderate* persistence, and $\rho(\tilde{\mathbf{A}}) \approx 0.95$ as *high* persistence. The scenario *hard constraints* treats the first three variables as missing and conditions on the realizations of the remaining variables; *soft constraint* restricts one of the variables to the predefined interval $(\mu_y - 0.1, \mu_y + 0.1)$ where $\mu_y = 1/h \sum_{t=T-h+1}^T y_{i,t}$, i.e., the mean of the respective variable over its final h in-sample periods.

The resulting conditional forecasts are shown in Figure 1. The solid grey lines mark the 68 percent credible set and the median of the predictive distribution when using our proposed recursive approach; the dashed navy blue lines show the same percentiles when using the precision sampler. Considering panels (a) and (b), when facing a moderate amount of persistence, the two approaches yield virtually identical estimates. Some deviations are visible in panels (c) and (d), especially for the left-most panel under the hard constraints and for the first two variables under the soft restriction. In the majority of

our experiments, the differences were practically negligible. But this is not necessarily the case in all conceivable scenarios.

3.2. Generalized impulse responses

The IRF is a ubiquitous object of interest in macroeconomics and is widely used for both academic and policy analysis. For the purposes of our paper, we follow the literature and define IRFs generically as:

$$\frac{\partial \mathbf{y}_{\tau+h}}{\partial u_{j\tau}} = \mathbb{E}(\mathbf{y}_{\tau+h} \mid \mathcal{I}, u_{j\tau} = d) - \mathbb{E}(\mathbf{y}_{\tau+h} \mid \mathcal{I}). \quad (10)$$

As their name suggests, IRFs trace the dynamic evolution of one or more variables in response to an exogenous structural shock impact (the “impulse”) of size d at time τ across horizons h , where the structural shock is encoded in $u_{j\tau}$. Conventional IRFs from (conditionally) linear VARs are symmetric and proportional with respect to the sign and size of shocks, and they are time-invariant, at least in the case of constant parameter VARs. By contrast, in nonlinear models such as those we consider in this paper, the sign, size, and timing of a shock may matter and can lead to nonlinearities in responses. Due to this state dependence, we cannot use standard methods but need to resort to GIRFs instead, see [Koop *et al.* \(1996\)](#). We discuss our implementation of GIRFs below and then extend the baseline framework to allow for studying various types of counterfactual shock and transmission scenarios.

The model outlined in Equation (1) is conditionally Gaussian, and standard approaches from the SVAR literature (e.g., zero/sign restrictions, instrumental/proxy variables) can be used to identify structural shocks. Suppose we have (either internally or externally) identified the impact of the structural shock $u_{j\tau}$ of size $d = 1$ on the endogenous variables of interest, $\partial \mathbf{y}_{\tau} / \partial u_{j\tau} = \boldsymbol{\delta}_0^{(m)}$ at iteration m . To sample from the posterior distribution of the GIRFs across horizons, we will use the conditionally Gaussian form of Equation (3). Our goal here is to compare factual and counterfactual scenarios, i.e., we want to compare the case when a structural shock occurs with a non-shock baseline scenario.

We construct these scenarios by first defining two distinct versions of initial conditions. In particular, $\mathbf{x}_{\tau+1}^{(m,d)} = ((\mathbf{y}_\tau + d\boldsymbol{\delta}_0^{(m)})', \mathbf{y}'_{\tau-1}, \dots, \mathbf{y}'_{\tau-p+1})'$, with superscript d indicating the shock scenario for each iteration m of our algorithm, and $\mathbf{x}_{\tau+1}^{(m,\emptyset)} = (\mathbf{y}'_\tau, \mathbf{y}'_{\tau-1}, \dots, \mathbf{y}'_{\tau-p+1})'$ with superscript \emptyset referring to the “no-shock” scenario, i.e., it uses the actual configuration of the input vector at time τ . Let \mathbf{J} be a $k \times n$ selection matrix which has an identity matrix in its upper $n \times n$ block and zeroes everywhere else.

The GIRF on impact reflects our desired shock scenario and is given by:

$$\boldsymbol{\lambda}_{\tau,0}^{(m,d)} = \mathbf{J}'(\mathbf{x}_{\tau+1}^{(m,d)} - \mathbf{x}_{\tau+1}^{(m,\emptyset)}) = d\boldsymbol{\delta}_0^{(m)}.$$

That is, we assume that the impact of the respective shock is constant over time, and shocks of different sizes can be simulated by setting d accordingly. Using Equation (4), we obtain two predictive distributions of interest:

$$\begin{aligned} p(\mathbf{y}_{\tau+1} \mid u_{j\tau} = d, \mathcal{I}, \boldsymbol{\Xi}^{(m)}) &= \mathbf{F}^{(m)}(\mathbf{x}_{\tau+1}^{(m,d)}) + \boldsymbol{\epsilon}_{\tau+1}, \\ p(\mathbf{y}_{\tau+1} \mid \mathcal{I}, \boldsymbol{\Xi}^{(m)}) &= \mathbf{F}^{(m)}(\mathbf{x}_{\tau+1}^{(m,\emptyset)}) + \boldsymbol{\epsilon}_{\tau+1}, \end{aligned}$$

where $\boldsymbol{\epsilon}_{\tau+1} \sim \mathcal{N}(\mathbf{0}_n, \boldsymbol{\Sigma}_{\tau+1}^{(m)})$. In line with the definition of an IRF in Equation (10), at horizon $h = 1$, we have $\boldsymbol{\lambda}_{\tau,1}^{(m,d)} = \mathbf{F}^{(m)}(\mathbf{x}_{\tau+1}^{(m,d)}) - \mathbf{F}^{(m)}(\mathbf{x}_{\tau+1}^{(m,\emptyset)})$. For higher-order responses $h \geq 2$, we may iterate forward, sampling from the distribution of the future (reduced form) shocks to obtain draws from the unconditional predictive distribution and the distribution conditioning on a shock at time τ for each horizon. Specifically, for $s \in \{d, \emptyset\}$ and analogous to Equation (5), we have $\mathbf{x}_{\tau+h}^{(m,s)} = (\mathbf{y}_{\tau+h-1}^{(m,s)'} , \mathbf{y}_{\tau+h-2}^{(m,s)'} , \dots)'$ and thus,

$$p(\mathbf{y}_{\tau+h} \mid u_{j\tau} = s, \mathcal{I}, \{\mathbf{y}_t^{(m,s)}\}_{t=\tau+1}^{\tau+h-1}, \boldsymbol{\Xi}^{(m)}) = \mathcal{N}(\mathbf{F}^{(m)}(\mathbf{x}_{\tau+h}^{(m,s)}), \boldsymbol{\Sigma}_{\tau+h}^{(m)}), \quad (11)$$

which we use to compute the GIRF at generic horizon h :

$$\begin{aligned}\boldsymbol{\lambda}_{\tau,h}^{(m,d)} &= \mathbb{E}(\mathbf{y}_{\tau+h} \mid \mathcal{I}, u_{j\tau} = d, \mathbf{y}_{\tau+1:\tau+h-1}^{(m,d)}, \boldsymbol{\Xi}^{(m)}) - \mathbb{E}(\mathbf{y}_{\tau+h} \mid \mathcal{I}, \mathbf{y}_{\tau+1:\tau+h-1}^{(m,\emptyset)}, \boldsymbol{\Xi}^{(m)}) \quad (12) \\ &= \mathbf{F}^{(m)}(\mathbf{x}_{\tau+h}^{(m,d)}) - \mathbf{F}^{(m)}(\mathbf{x}_{\tau+h}^{(m,\emptyset)}).\end{aligned}$$

Two main comments about this framework are in order. First, for the case when \mathbf{F} is a linear function, our approach produces conventional IRFs. Second, when \mathbf{F} is nonlinear, one cannot apply expectations as straightforwardly as in the linear case. The reason is that when applying the logic of standard recursive substitutions in this context, the presence of nonlinearities complicates the moments of higher-order responses. For instance, taking $h = 2$ as an example, when \mathbf{F} is a linear mapping with associated (companion form) coefficients, $\tilde{\mathbf{A}}$, we obtain $\mathbb{E}(\tilde{\mathbf{A}}^2 \mathbf{x}_{\tau+1} + \tilde{\mathbf{A}} \boldsymbol{\epsilon}_{\tau+1} + \boldsymbol{\epsilon}_{\tau+2}) = \tilde{\mathbf{A}}^2 \mathbf{x}_{\tau+1}$. That is, the IRF at horizon h is given by $\mathbf{J}' \tilde{\mathbf{A}}^h (\mathbf{x}_{\tau+1}^{(m,d)} - \mathbf{x}_{\tau+1}^{(m,\emptyset)})$ where $\mathbf{x}_{\tau+1}^{(m,d)} - \mathbf{x}_{\tau+1}^{(m,\emptyset)} = (d \boldsymbol{\delta}_0^{(m)'}, \mathbf{0}'_{n(p-1)})'$, and can be obtained by simply projecting the shock impact forward using powers of $\tilde{\mathbf{A}}$. Since d can be factored out and the initial conditions cancel, the IRFs are time-invariant, symmetric, and proportional for different shock sizes and signs. By contrast, in a more general and possibly nonlinear context, this is clearly not the case since we obtain $\mathbb{E}[\mathbf{F}(\mathbf{F}(\mathbf{x}_{\tau+1} + \boldsymbol{\epsilon}_{\tau+1})) + \boldsymbol{\epsilon}_{\tau+2}] \neq \mathbf{F}(\mathbf{F}(\mathbf{x}_{\tau+1}))$, that is, e.g., at $h = 2$ the shock dated $\tau + 1$ enters nonlinearly, and so on.

Equation (12) thus addresses the reduced form shocks that enter nonlinearly to obtain the respective conditional expectation (implicitly via the recursive simulation of the factual and counterfactual paths of the variables $\mathbf{y}_{\tau+1:\tau+h-1}^{(m,s)}$). Computing $\boldsymbol{\lambda}_{\tau,h}^{(m,d)}$ for each iteration m allows us to explore the posterior of the expression in Equation (10). Notably, we obtain a GIRF across horizons $h = 0, 1, 2, \dots$, for each point in time τ . In principle, one may thus consider dynamic time-varying effects of shocks for different subsets of observations (e.g., recessions vs. expansions), or for each period individually. For most of our empirical work, we will focus on simple time averages $\bar{\boldsymbol{\lambda}}_h^{(m,d)} = 1/T \sum_{\tau=1}^T \boldsymbol{\lambda}_{\tau,h}^{(m,d)}$, and thus abstract from this dimension of asymmetry.

Another possibility for that we explore in our applied work combines our approach to

conditional forecasts with our algorithm for computing GIRFs. Specifically, we may switch off specific transmission channels of structural shocks by partially matching the moments of the predictive distribution conditional on the shock with those of the unconditional predictive distribution. By construction, this results in a GIRF that is equal to zero for the restricted dimensions, thereby effectively considering an alternative scenario where the shock cannot propagate through this channel. From an implementation perspective, we may manipulate Equation (11) for $s = d$ using a hard restriction as in Equation (9), such that $\mathbf{r}_h^{(m)} = \mathbf{R}_h \mathbf{F}^{(m)}(\mathbf{x}_{\tau+h}^{(m,\varnothing)})$. That is, we impose that $\mathbf{R}_h \boldsymbol{\lambda}_{\tau,h}^{(m,d)} = \mathbf{0}_{r_h}$ along the desired r_h dimensions.

4. EMPIRICAL APPLICATIONS

We employ the proposed framework in three related yet distinct applications. First, we use the annual stress test scenarios conducted by the Federal Reserve System and compute conditional forecasts using soft constraints on several variables. Second, we study the implications of varying financial conditions (imposing hard constraints over a period) on tail risks of output growth, inflation, and employment. Third, we identify a US-based financial shock and gauge the role of spillovers and spillbacks to several other major economies. Across these applications we mainly compare a *homoskedastic* (BART-hom, setting $s_t = 1$ for all t) and *heteroskedastic* BART implementation (BART-het) with a *heteroskedastic* BVAR (BVAR-het), both of which feature the outlier specification. Due to our sample featuring the Covid-19 pandemic observations we disregard the homoskedastic BVAR version (see [Lenza and Primiceri, 2022](#), for a discussion).

4.1. Stress testing scenarios for the US economy

In our first application, we conduct a scenario analysis for the US economy inspired by the 2024 version of the *Dodd-Frank Act* (DFA) stress test assumptions. This annual stress test is conducted and published by the Board of Governors of the Federal Reserve System. Details about the underlying dataset are provided in [Appendix A](#). The information set

features about 25 broad variables (capturing economic activity, the labor market, prices, housing and the financial sector). We estimate our models using data on a quarterly frequency ranging from 1976Q1 to 2023Q4, and subsequently consider a baseline and adverse scenario for the period from 2024Q1 to 2027Q1. These scenarios are imposed via soft constraints on the future path of the unemployment rate (UNRATE), CPI inflation (CPIAUCSL), and 10-year government bond yields (GS10), similar to Chan *et al.* (2025). They are visualized in Figure 2.

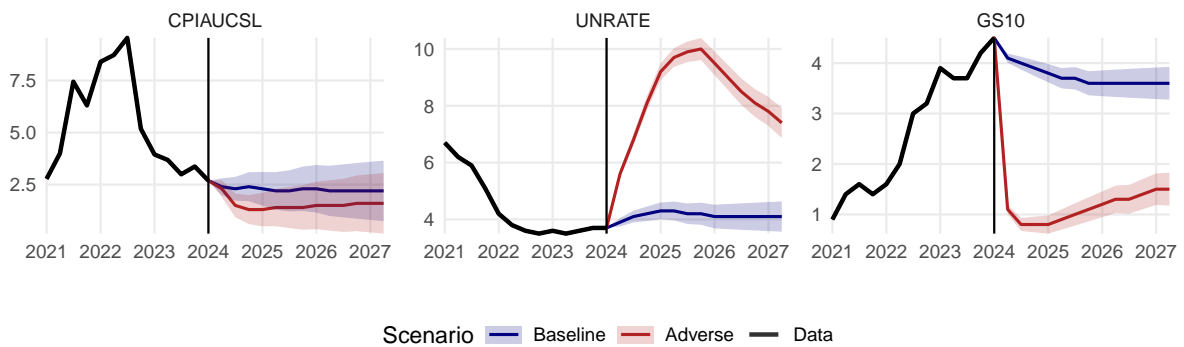


Figure 2: Restrictions imposed on the future paths of the indicated variables.

Notes: Scenarios according to the 2024 DFA stress test assumptions (solid lines), shaded areas indicate the bounds of the imposed soft restrictions. Variables: Consumer price inflation (CPIAUCSL), unemployment rate (UNRATE), and 10-year government bond yields (GS10).

We display the posterior median forecasts alongside 50 and 68 percent posterior credible sets for selected unrestricted variables in Figure 3: real GDP (GDPC1), industrial production (INDPRO), personal consumption expenditure (PCE) inflation (PCECTPI), payroll employment (PAYEMS), 1-year government bond yields (GS1) and the Gilchrist and Zakrajšek (2012) excess bond premium (EBP). The baseline scenario draws from the consensus projections from 2024 *Blue Chip Financial Forecasts* and *Blue Chip Economic Indicators*. The adverse scenario is characterized by a severe recession. It is noteworthy that the unconditional forecasts (in grey shades) approximately coincide with the baseline scenario (blue shades) in most cases. This is unsurprising, given that this scenario is designed to reflect the expectations of market participants, who apparently predict the economy to evolve similarly to what the models we consider here predict. Differences emerge irrespective of the linear vs. nonlinear specification for short-term interest rates,

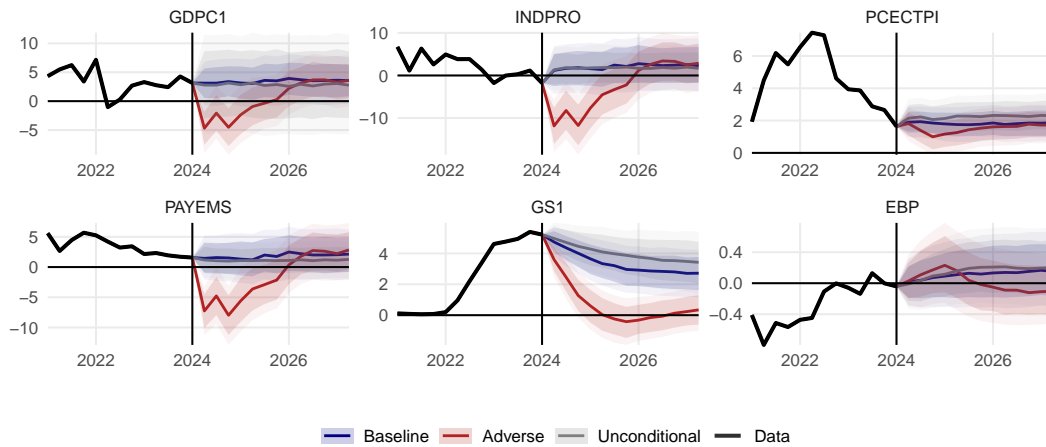
which are predicted to stay at a somewhat higher level unconditionally; and the BVAR suggests inflation to be elevated when comparing the unconditional forecast to the baseline scenario.

Turning to the adverse scenario, a different picture emerges — specifically, the scenario forecasts differ significantly from the unconditional forecasts. And there are some differences arising from nonlinearities in both the conditional means and variances. Interestingly, the different model specifications mostly agree about path of PCE inflation, financial conditions and the short-term interest rate conditional on the adverse scenario. As expected, financial conditions tighten initially but tend to improve subsequently, partially through a monetary easing response by the central bank as reflected in short-term interest rates. In addition, the assumed trajectory of the conditioning variables results in a modestly disinflationary episode that vanishes by 2026.

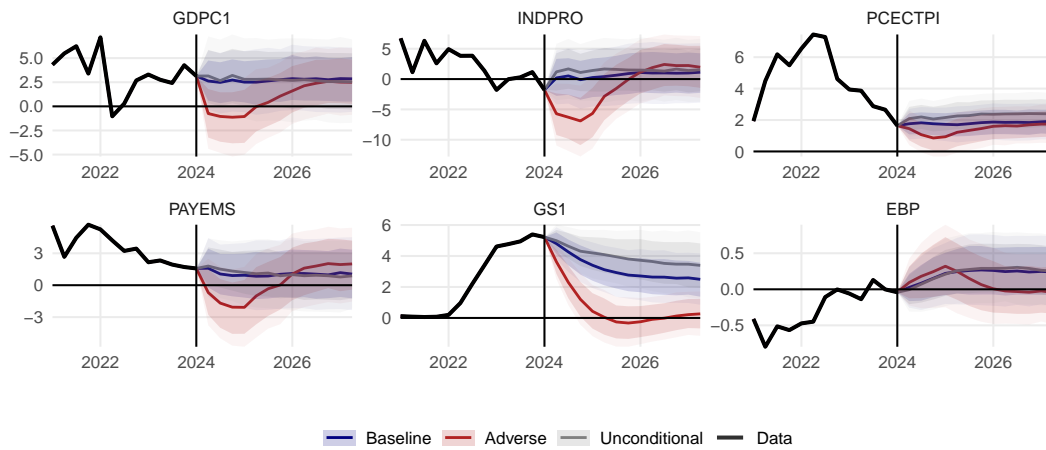
Major differences across model implementations emerge when considering measures of economic activity and payroll employment. While all three models agree about the fact that the adverse scenario leads to a significant economic contraction, the heteroskedastic BART model suggests somewhat less severe magnitudes of this downturn. This can be explained by noting that for this specification, the algorithm decides to classify several observations (that are otherwise informative about directional movements of variables when assuming homoskedasticity) as noisy or even outliers. We note that BART, due to the way how tree-based approaches fit data, is capable of dealing with outliers and heteroskedastic data features in the conditional mean function by design (see [Huber *et al.*, 2023](#); [Clark *et al.*, 2023](#), for discussions), even when assuming homoskedastic reduced form errors. But in this case it classifies several observations instead as noise rather than signal.

Comparing the homoskedastic BART-version with the BVAR, which are closer in terms of conditional predictive distributions for the adverse scenario, both suggest a significant decline in industrial production, with a trough at -10 percent (about -6 percent for heteroskedastic BART). Relatedly, the BVAR predicts a decline in real GDP of about -4 percent, roughly in line with the numbers obtained when running homoskedastic BART, at -5 percent. Where the two differ in this context is in the predicted recovery following

(a) BART-hom



(b) BART-het



(c) BVAR-het

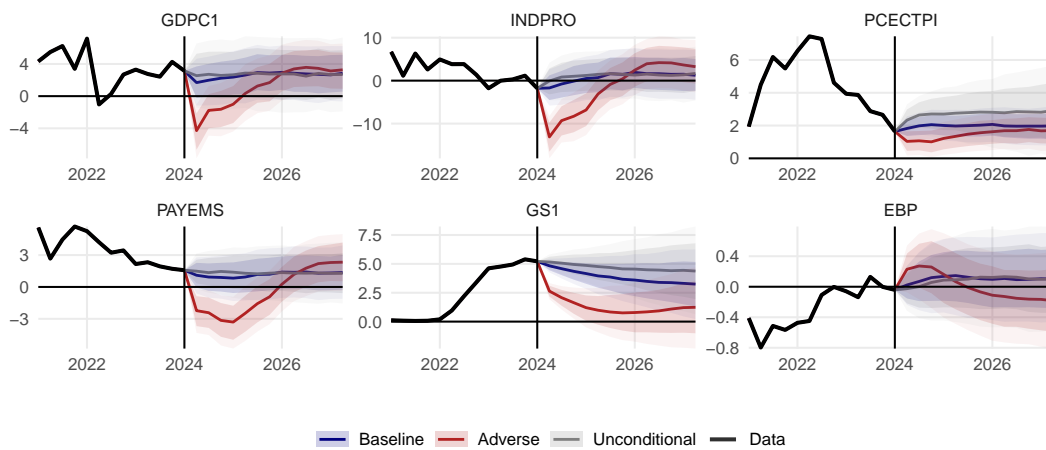


Figure 3: Conditional and unconditional forecasts for selected variables.

Notes: Posterior median alongside 50/68 percent credible sets. Variables: Real GDP (GDPC1), industrial production (INDPRO), personal consumption expenditure inflation (PCECTPI), payroll employment (PAYEMS), 1-year government bond yields (GS1) and excess bond premium (EBP).

the trough, which is more sluggish for the nonparametric model. Turning to payroll employment, homoskedastic BART suggests a sharper decline of about -6 percent, which is about twice the size of the decline conditionally forecasted by the heteroskedastic BART and BVAR models.

4.2. Financial conditions in the US and tail risk scenarios

In this empirical application, we restrict our sample from 1976Q1 to 2017Q4 and consider the period from 2018Q1 until 2019Q1 as a laboratory to assess nonlinearities in the relationship between economic variables and financial conditions. For this application we use the homoskedastic BART model as the pandemic observations are excluded from our dataset. We investigate nonlinear patterns of macroeconomic risk, which, following the “growth-at-risk” approach of [Adrian *et al.* \(2019\)](#), is defined as the predictive quantiles of some variable of interest at a pre-defined probability level (in line with value-at-risk, VaR, in finance). We pick this period because the information set already contains the global financial crisis (and the model thus had the opportunity to learn from this severe financial episode), and because this “holdout sample” otherwise coincides with a comparatively eventless period. We impose hard constraints on the future path of the National Financial Conditions Index (NFCI) and trace the effects of these scenarios on several macroeconomic variables. The scenarios are defined to reflect an increase of the NFCI ranging from approximately 1, 3 and 6 unconditional standard deviations (reflecting tighter financial conditions) in 2018Q1, which we implement by placing these values as hard restriction on the NFCI in that quarter. From 2018Q2 onward we leave the respective future path unrestricted.

We investigate growth-at-risk (quantiles of real GDP), inflation-at-risk (quantiles of PCE inflation) and labor-at-risk (quantiles of growth in payroll employment) as our objects of interest (see [Adams *et al.*, 2021](#); [Botelho *et al.*, 2024](#); [Clark *et al.*, 2024](#); [Lopez-Salido and Loria, 2024](#), for related papers). The resulting conditional forecast distributions (density estimates) are shown in Figure 4. Computing the difference between these condi-

tional scenario distributions and the unconditional one yields an estimate of the unorthogonalized IRF (UIRF). In the spirit of Equation (10), we have $\mathbb{E}(\mathbf{y}_{\tau+h}|\mathcal{I}, \mathcal{C}_{1:h}) - \mathbb{E}(\mathbf{y}_{\tau+h}|\mathcal{I})$, which is the counterfactual difference between the scenario defined by the restrictions in the \mathcal{C}_h 's and the unconditional forecast. Different to a simulation of an individual structural shock, the UIRF reflects a likely combination of structural shocks that increases the NFCI by a predefined amount, see also Crump *et al.* (2025).

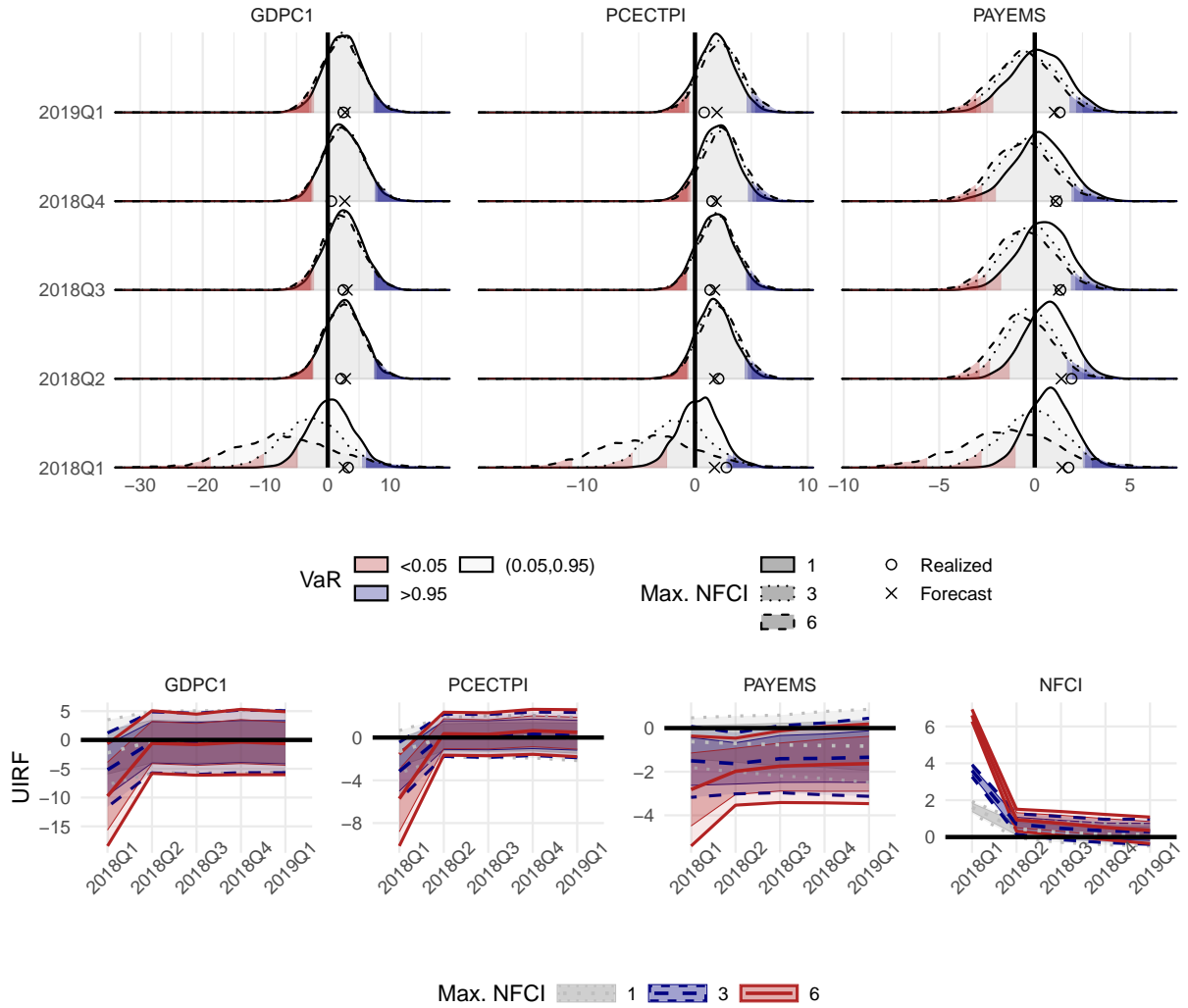


Figure 4: Conditional forecast distributions for selected variables and macroeconomic value-at-risk (VaR) for different scenarios of financial stress.

Notes: The crosses mark the posterior median for unconditional forecasts and circles indicate realized values. Max. NFCI refers to the maximum value of the NFCI for the scenarios, with moderate (1), severe (3, comparable to the global financial crisis), and extreme stress (6). Sampling period 1976Q1 to 2017Q4, the hard restriction applies for 2018Q1. Unorthogonalized impulse response functions (UIRFs) are computed as the difference between the conditional and unconditional distribution (posterior median alongside 50 and 68 percent credible sets). Variables: Real GDP (GDPC1), personal consumption expenditure inflation (PCECTPI), payroll employment (PAYEMS), national financial conditions index (NFCI).

The different NFCI scenarios for 2018Q1 shift the predictive distributions, especially during the quarter when this reduced form shock materializes. The resulting dynamic effects, as measured with the UIRFs, are rather short-lived for real GDP and PCE inflation, but more persistent for payroll employment. In all shown cases, the economy contracts which is reflected in a decrease of real GDP growth and payroll employment, and the simulated shock has a deflationary effect. A clear pattern that emerges is that while the upper tails of the distributions remain rather stable (upside risk is constant), downside risk as measured by the lower quantiles increases significantly for all considered variables (the red shaded VaR < 0.05 moves strongly leftwards), and there are some visible asymmetries. While the moderate NFCI scenario (max. NFCI = 1) results in growth-at-risk for the 5th percentile at about -5 percent, the severe (max. NFCI = 3) and extreme (max. NFCI = 6) stress scenarios yield -10 and -20 percent, respectively. This finding is also present for inflation-at-risk and labor-at-risk.

The resulting predictive distributions exhibit non-Gaussian features, chief among them being particularly heavy tails and skewness (see also Clark *et al.*, 2023, for a related but simplified scenario analysis in this context). In addition, there are hints of multimodality as the assumed values for the NFCI in 2018Q1 turn more extreme, which relates to the discussions in Adrian *et al.* (2021). For instance, while most mass of the predictive distribution of payroll employment growth, for the extreme stress scenario, is centered on about -3 percent, there is a smaller local peak at values of -5 percent. A similar pattern is visible for PCE inflation.

4.3. Spillovers and spillbacks of US financial shocks

This application estimates the effect of a financial shock in the US and traces its effects through the domestic economy, but also captures spillovers and spillbacks to and from several other economies. We use a slightly different dataset in this case, which drops several of the domestic indicators, but adds bilateral exchange rates with the EA and Japan alongside real GDP for the EA, Japan and the UK.

Following the SVAR literature, we assume that the reduced form shocks are linked to the structural shocks as follows, $\boldsymbol{\epsilon}_t = \mathbf{A}_0^{-1} \mathbf{u}_t$. This implies that $\boldsymbol{\Sigma} = \mathbf{A}_0^{-1} \mathbf{A}_0^{-1'}$, and we identify \mathbf{A}_0^{-1} using a set of zero impact restrictions imposed with a Cholesky decomposition of the form $\boldsymbol{\Sigma} = \mathbf{D}\mathbf{D}'$. That is, $\mathbf{A}_0^{-1} = \mathbf{D}$ and $\partial \mathbf{y}_\tau / \partial u_{j\tau} = \mathbf{D}\mathbf{e}'_j = \boldsymbol{\delta}_0$ and we orthogonalize the structural shocks (different to the application in Section 4.2 which dealt with unorthogonalized shocks that resulted in an increase of the NFCI). We simulate different shock sizes of different signs with $d \in \{-3, -1, 1, 3, 6\}$. Different to conventional linear SVAR frameworks, our approach allows to assess nonlinearities of responses with respect to different signs and magnitudes of a shock with GIRFs. Such asymmetries and related nonlinearities have recently gained attention both in a VAR and local projection context, see, e.g., Mumtaz and Piffer (2022); Carriero *et al.* (2023); Forni *et al.* (2024); Hauzenberger *et al.* (2024a).

To identify the financial shock, we place timing-restrictions on the contemporaneous impulse responses as described above. This is operationalized with a specific ordering of the quantities in the vector \mathbf{y}_t . Specifically, we structure this vector such that all slow moving domestic and foreign macroeconomic variables come first (which imposes zero restrictions on impact). These variables are then followed by the excess bond premium (EBP, Gilchrist and Zakrajšek, 2012), and all fast moving variables such as those capturing the financial economy. We interpret the orthogonalized innovation of the EBP equation as the financial shock, similar to Barnichon *et al.* (2022). In a multicountry context, Huber *et al.* (2024) use an identification scheme virtually identical to ours.

We present selected results for key macroeconomic and financial variables in Figure 5, additional empirical results can be found in the Appendix. While our framework allows to compute GIRFs for each period in our sample, we focus on time averages in the results that follow. The rows in the figure show different subsets of the same set of results, structured such that the shocks of different signs and sizes can be compared with ease. That is, for visualization purposes, we typically rescale the GIRFs to a common range by computing “normalized” GIRFs, $\tilde{\boldsymbol{\lambda}}_{\tau,h}^{m,d} = \boldsymbol{\lambda}_{\tau,h}^{(m,d)} / d$. Note that for linear VARs, such scalings do not make a difference because the responses are symmetric (see the additional

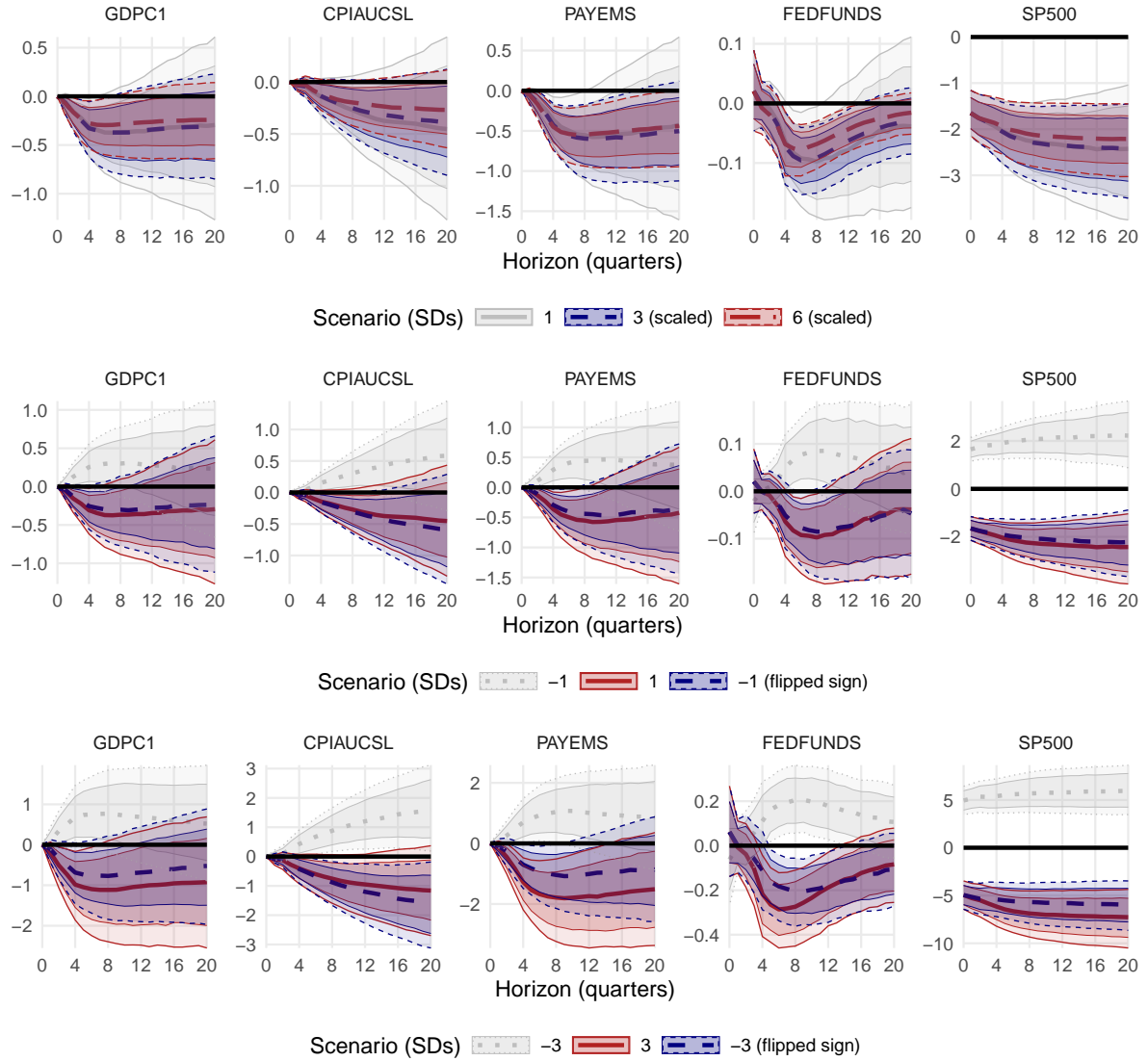


Figure 5: Impulse response functions for selected variables to a financial shock in the US, comparing asymmetries due to size and sign of the shocks.

Notes: Posterior median alongside 50 and 68 percent credible sets. Cumulated responses for variables in differences and levels for all other variables. Variables: Real GDP (GDPC1), consumer price inflation (CPIAUCSL), payroll employment (PAYEMS), federal funds rate (FEDFUNDS) and S&P500 index (SP500).

results for the linear BVAR in the Appendix). For nonlinear models, this is not necessarily the case and allows for a visual inspection of asymmetries.

Starting with the first row in Figure 5, we find that the size of the financial shock does not matter much for the GIRFs about any of the indicated variables. Financial shocks of different sizes rescaled to reflect a 1 standard deviation innovation rather symmetrically decrease real GDP and payroll employment. Peak effects occur between one and two years after impact of the shock. In addition, the shock puts a persistent downward pressure

on prices and leads to a decline in the Federal funds rate which peaks at about -10 basis points after around a year. Notably it does not react on impact, different to stock returns which immediately decline by about 1.5 percent during the quarter that the shock materializes. Qualitatively and in terms of magnitudes, these estimates are roughly in line with those in [Gilchrist and Zakrajšek \(2012\)](#). We do not report these results here to save space, but note that the US-based financial shock spills over to the other economies and leads to contractionary effects in terms of real GDP.

Having established that the size of the financial shock does not seem to matter much, the second and third row zoom into sign asymmetries. Here, we show the raw GIRF in grey, while a version of the normalized GIRF flips the sign to ease comparisons. The 1 standard deviation US-based financial shock does not result in significant sign asymmetries (the posterior distributions overlap for the most part). Turning to the final row, this clearly differs for larger sized shocks of different signs. For these GIRFs that show the responses to a positive and negative 3 standard deviation shock, asymmetries are striking and significant for most variables. In particular, we find that the negative effect on payroll employment is almost twice as large for adverse shocks, and the Federal Reserve responds more strongly to adverse financial shocks, as measure with the much stronger shift in the Federal funds rate. These findings corroborate the empirical evidence presented by the preceding literature (see, e.g., [Forni *et al.*, 2024](#); [Hauzenberger *et al.*, 2024a](#)).

We next explore the role of international variables in the domestic transmission of the US shock. For this purpose, besides unrestricted GIRFs, we consider an alternative analysis where non-domestic transmission channels are switched off. This is different to [Huber *et al.* \(2024\)](#), who focus on international effects of US-based shocks; indeed, we investigate how international channels affect the domestic transmission of shocks originating in the US. That is, we impose the restriction that foreign variables do not respond to the financial shock in the US in this counterfactual, thereby simulating a scenario where the financial shock is fully confined to the domestic economy without any spillovers (or spillbacks); see [Breitenlechner *et al.* \(2022\)](#) for a monetary application in this context.

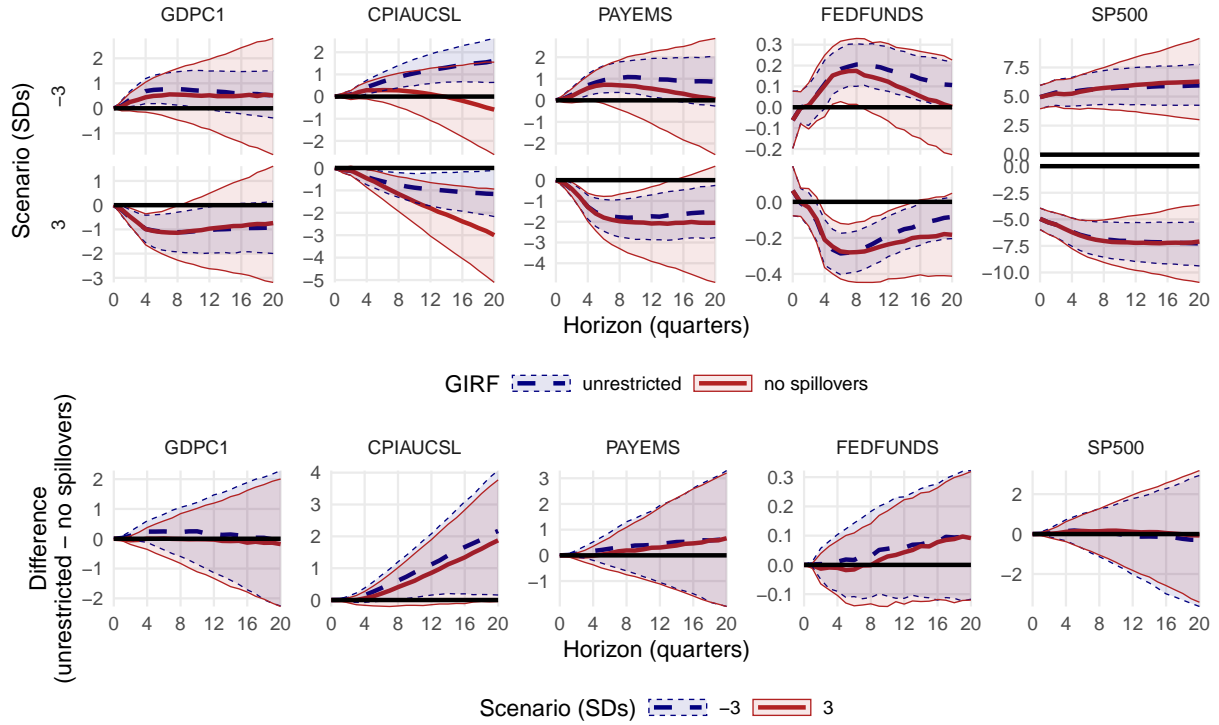


Figure 6: Unrestricted and restricted impulse response functions for selected variables.

Notes: The restricted case assumes that the US financial shock does not spill over to non-domestic variables. The upper panels show the GIRFs for these two cases, and the lower panel shows the posterior distribution of the differences between the unrestricted and no-spillovers scenario. Posterior medians alongside 50 percent credible sets. Cumulated responses for variables in differences and levels for all other variables.

The results are displayed in Figure 6. The upper panels show the unrestricted GIRFs (those shown and discussed in the context of Figure 5) and restricted “no spillovers” GIRFs. The lower panels plot the difference between the two. Two key findings are worth reporting. First, for the most part, ruling out spillovers and spillbacks does not significantly alter the GIRFs for most variables. This can be observed from the credible sets covering the zero line in all but one panel in the bottom row of the figure. Second, international transmission channels appear to matter for inflation dynamics after financial shocks. We find that in the no-spillover case, the restricted GIRFs to the shocks of different signs are clearly asymmetric. The inflation response is insignificant for benign financial shocks, but significantly negative for adverse shocks; this is different for unrestricted GIRFs, which are mostly symmetric.

In terms of the importance of international transmission channels for the domestic

shock propagation, we find that non-domestic dynamics partially offset disinflationary or deflationary pressures in response to adverse US financial shocks. By contrast, in the no-spillover case, the inflation GIRFs take smaller or even negative values for benign financial shocks than in the unrestricted case. These patterns suggests that propagation through non-domestic variables overall lowers the inflation responses irrespective of the sign of the shock. In other words, ruling out international channels loosely speaking introduces a negative “bias” of the response of US inflation in this counterfactual simulation.

5. CONCLUSIONS

This paper presents a robust and unified methodology for conducting scenario analysis in multivariate macroeconomic settings, accommodating nonlinearities and unknown functional forms of conditional mean relationships. The proposed methods are applicable not only in traditional nonlinear frameworks, such as variants of threshold or time-varying parameter models, but also to more recently developed models incorporating machine learning techniques. By extending conditional forecasts and GIRFs to a flexible, non-parametric framework, we address some limitations of traditional linear and parametric models in generating various types of counterfactual analyses. Specifically, we explore the application of conditional forecasts in a nonlinear setting by leveraging the properties of conditionally Gaussian errors. Furthermore, we demonstrate how to derive dynamic causal effects in the form of GIRFs in a nonlinear context and quantify the contribution of specific transmission channels in the propagation of structural shocks. This approach is broadly applicable and computationally efficient, making it suitable for large-scale macroeconomic datasets.

Empirical applications, focusing on the use of BART as an example of nonparametric modeling of the conditional mean function, underscore the critical role of nonlinearities and heteroskedasticity in shaping macroeconomic dynamics. For instance, scenario analysis based on Federal Reserve stress tests reveals differences between linear and nonlinear models in forecasting economic contractions and recoveries. Similarly, our growth-at-risk

application demonstrates how nonlinearities influence the distribution of macroeconomic risks under financial stress, particularly in amplifying downside risks. Finally, the analysis of financial spillovers reveals significant asymmetries in the transmission of shocks and the influence of international linkages on domestic outcomes. Our results indicate that incorporating nonlinearities in conditional forecasts and scenario analysis provides a richer understanding of risk propagation and policy effects. By addressing limitations in traditional linear approaches and offering a flexible tool for analyzing complex economic relationships, this paper contributes to the literature on macroeconomic forecasting, risk assessment, and policy evaluation.

REFERENCES

- ADAMS PA, ADRIAN T, BOYARCHENKO N, AND GIANNONE D (2021), “Forecasting macroeconomic risks,” *International Journal of Forecasting* **37**(3), 1173–1191.
- ADRIAN T, BOYARCHENKO N, AND GIANNONE D (2019), “Vulnerable growth,” *American Economic Review* **109**(4), 1263–1289.
- (2021), “Multimodality in macrofinancial dynamics,” *International Economic Review* **62**(2), 861–886.
- ANTOLIN-DIAZ J, PETRELLA I, AND RUBIO-RAMÍREZ JF (2021), “Structural scenario analysis with SVARs,” *Journal of Monetary Economics* **117**, 798–815.
- BAÑBURA M, GIANNONE D, AND LENZA M (2015), “Conditional forecasts and scenario analysis with vector autoregressions for large cross-sections,” *International Journal of Forecasting* **31**(3), 739–756.
- BARNICHON R, MATTHES C, AND ZIEGENBEIN A (2022), “Are the effects of financial market disruptions big or small?” *Review of Economics and Statistics* **104**(3), 557–570.
- BOTELHO V, FORONI C, AND RENZETTI A (2024), “Labour at risk,” *European Economic Review* **170**, 104849.
- BOTEV ZI (2017), “The normal law under linear restrictions: simulation and estimation via minimax tilting,” *Journal of the Royal Statistical Society (Series B)* **79**(1), 125–148.
- BREITENLECHNER M, GEORGIADIS G, AND SCHUMANN B (2022), “What goes around comes around: How large are spillbacks from US monetary policy?” *Journal of Monetary Economics* **131**, 45–60.
- CARRIERO A, CLARK TE, AND MARCELLINO M (2016), “Common drifting volatility in large Bayesian VARs,” *Journal of Business & Economic Statistics* **34**(3), 375–390.
- CARRIERO A, CLARK TE, MARCELLINO M, AND MERTENS E (2023), “Shadow-rate VARs,” *Deutsche Bundesbank DP* **14/2023**.
- (2024), “Addressing COVID-19 outliers in BVARs with stochastic volatility,” *Review of Economics and Statistics* 1–15.
- CHAN JC (2020), “Large Bayesian VARs: A flexible Kronecker error covariance structure,” *Journal of Business & Economic Statistics* **38**(1), 68–79.

- (2023), “Comparing stochastic volatility specifications for large Bayesian VARs,” *Journal of Econometrics* **235**(2), 1419–1446.
- CHAN JC, PETTENUZZO D, POON A, AND ZHU D (2025), “Conditional Forecasts in Large Bayesian VARs with Multiple Equality and Inequality Constraints,” *Journal of Economic Dynamics and Control* **105061**.
- CHAN JC, POON A, AND ZHU D (2023), “High-dimensional conditionally Gaussian state space models with missing data,” *Journal of Econometrics* **236**(1), 105468.
- CHIPMAN HA, GEORGE EI, AND MCCULLOCH RE (2010), “BART: Bayesian additive regression trees,” *The Annals of Applied Statistics* **4**(1), 266–298.
- CLARK TE, HUBER F, KOOP G, MARCELLINO M, AND PFARRHOFER M (2023), “Tail forecasting with multivariate Bayesian additive regression trees,” *International Economic Review* **64**(3), 979–1022.
- (2024), “Investigating growth-at-risk using a multicountry nonparametric quantile factor model,” *Journal of Business & Economic Statistics* **42**(4), 1302–1317.
- CONG Y, CHEN B, AND ZHOU M (2017), “Fast simulation of hyperplane-truncated multivariate normal distributions,” *Bayesian Analysis* **12**(4), 1017–1037.
- CRUMP RK, EUSEPI S, GIANNONE D, QIAN E, AND SBORDONE AM (2025), “A large Bayesian VAR of the United States economy,” *International Journal of Central Banking* **forthcoming**.
- DOAN T, LITTERMAN R, AND SIMS C (1984), “Forecasting and conditional projection using realistic prior distributions,” *Econometric reviews* **3**(1), 1–100.
- ESSER J, MAIA M, PARNELL AC, BOSMANS J, VAN DONGEN H, KLAUSCH T, AND MURPHY K (2024), “Seemingly unrelated Bayesian additive regression trees for cost-effectiveness analyses in healthcare,” *arXiv* **2404.02228**.
- FISCHER MM, HAUZENBERGER N, HUBER F, AND PFARRHOFER M (2023), “General Bayesian time-varying parameter vector autoregressions for modeling government bond yields,” *Journal of Applied Econometrics* **38**(1), 69–87.
- FORNI M, GAMBETTI L, MAFFEI-FACCIOLI N, AND SALA L (2024), “Nonlinear transmission of financial shocks: Some new evidence,” *Journal of Money, Credit and Banking* **56**(1), 5–33.
- GILCHRIST S, AND ZAKRAJŠEK E (2012), “Credit spreads and business cycle fluctuations,” *American Economic Review* **102**(4), 1692–1720.
- GOULET COULOMBE P (2024), “To bag is to prune,” *Studies in Nonlinear Dynamics & Econometrics* **forthcoming**.
- GOULET COULOMBE P, LEROUX M, STEVANOVIC D, AND SURPRENANT S (2022), “How is machine learning useful for macroeconomic forecasting?” *Journal of Applied Econometrics* **37**(5), 920–964.
- HAUZENBERGER N, HUBER F, KLIEBER K, AND MARCELLINO M (2024a), “Machine Learning the Macroeconomic Effects of Financial Shocks,” *arXiv* **2412.07649**.
- HAUZENBERGER N, HUBER F, AND KOOP G (2024b), “Macroeconomic forecasting using BVARs,” in MP CLEMENTS, AND AB GALVÃO (eds.) “Handbook of Research Methods and Applications in Macroeconomic Forecasting,” chapter 2, 15–42, Cheltenham, UK/Northampton, USA: Edward Elgar Publishing.
- HAUZENBERGER N, HUBER F, MARCELLINO M, AND PETZ N (2024c), “Gaussian process vector autoregressions and macroeconomic uncertainty,” *Journal of Business & Economic Statistics* 1–17.
- HUANG A, AND WAND MP (2013), “Simple marginally noninformative prior distribu-

- tions for covariance matrices,” *Bayesian Analysis* **8**(2), 439–452.
- HUBER F, KLIEBER K, MARCELLINO MG, ONORANTE L, AND PFARRHOFER M (2024), “Asymmetries in International Financial Spillovers,” *SSRN* **5054831**.
- HUBER F, KOOP G, ONORANTE L, PFARRHOFER M, AND SCHREINER J (2023), “Nowcasting in a pandemic using non-parametric mixed frequency VARs,” *Journal of Econometrics* **232**(1), 52–69.
- HUBER F, AND ROSSINI L (2022), “Inference in Bayesian additive vector autoregressive tree models,” *The Annals of Applied Statistics* **16**(1), 104–123.
- JAROCIŃSKI M (2010), “Conditional forecasts and uncertainty about forecast revisions in vector autoregressions,” *Economics Letters* **108**(3), 257–259.
- KOOP G, PESARAN MH, AND POTTER SM (1996), “Impulse response analysis in non-linear multivariate models,” *Journal of Econometrics* **74**(1), 119–147.
- LENZA M, AND PRIMICERI GE (2022), “How to estimate a vector autoregression after March 2020,” *Journal of Applied Econometrics* **37**(4), 688–699.
- LOPEZ-SALIDO D, AND LORIA F (2024), “Inflation at risk,” *Journal of Monetary Economics* 103570.
- MARCELLINO M, AND PFARRHOFER M (2024), “Bayesian nonparametric methods for macroeconomic forecasting,” in MP CLEMENTS, AND AB GALVÃO (eds.) “Handbook of Research Methods and Applications in Macroeconomic Forecasting,” chapter 5, 90–125, Cheltenham, UK/Northampton, USA: Edward Elgar Publishing.
- MEDEIROS MC, VASCONCELOS GF, VEIGA Á, AND ZILBERMAN E (2021), “Forecasting inflation in a data-rich environment: the benefits of machine learning methods,” *Journal of Business & Economic Statistics* **39**(1), 98–119.
- MUMTAZ H, AND PIFFER M (2022), “Impulse response estimation via flexible local projections,” *arXiv* **2204.13150**.
- WAGGONER DF, AND ZHA T (1999), “Conditional forecasts in dynamic multivariate models,” *Review of Economics and Statistics* **81**(4), 639–651.

Online Appendix: Scenario analysis with multivariate Bayesian machine learning models

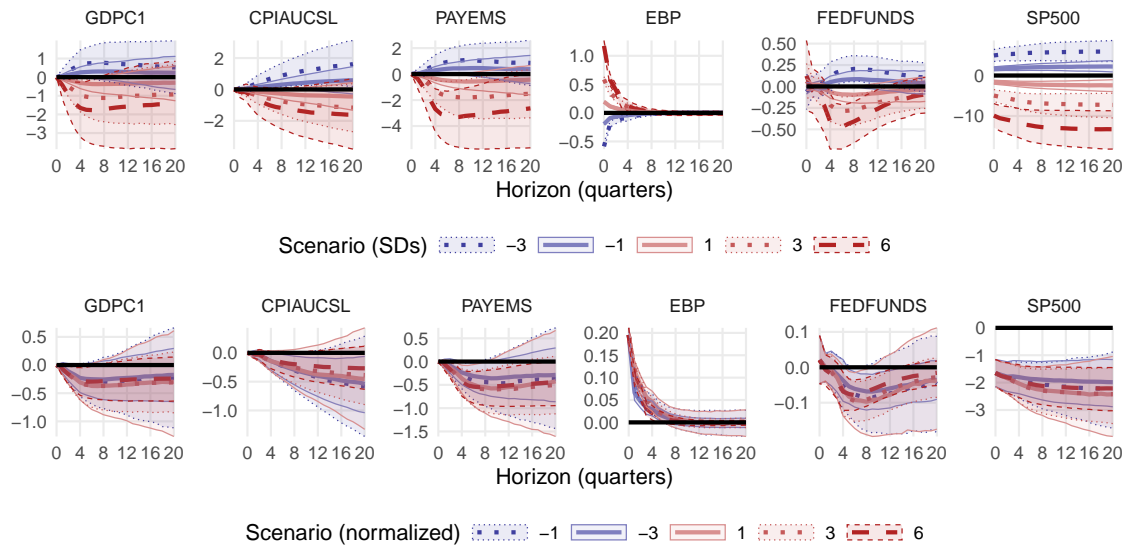
A. DATA

Table A.1: Dataset. *Notes:* Variable codes, descriptions and transformation: (0) no transformation $h(x_t) = x_t$; (1) annualized log-differences $h(x_t) = 400 \cdot \log(x_t/x_{t-1})$; (2) log-differences $h(x_t) = 100 \cdot \log(x_t/x_{t-1})$. Check marks indicate inclusion in the information sets for our applications (CF for Sections 4.1 and 4.2, GIRF for Section 4.3).

Code	Description	$h(x_t)$	CF	GIRF
GDPC1	Real gross domestic product	1	✓	✓
PCECC96	Real personal consumption expenditure	1	✓	
PRFIx	Real private fixed investment (residential)	1	✓	
GCEC1	Real Government consumption and investment	1	✓	
RDI	Real disposable income	0	✓	
INDPRO	Industrial production	1	✓	
CPIAUCSL	Headline consumer price index (CPI)	1	✓	✓
CPILFESL	Core CPI (excl. food and energy)	1	✓	
PCECTPI	Headline PCE prices	1	✓	
PCEPILFE	Core PCE prices (excl. food and energy)	1	✓	
HPI	House price index	1	✓	✓
HOUST	Housing starts	1	✓	
MR	Mortgage rate	0	✓	
PAYEMS	Payroll employment	1	✓	✓
UNRATE	Unemployment rate	0	✓	
FEDFUNDS	Federal funds rate	0	✓	✓
GS1	1-year treasury rate	0	✓	✓
GS10	10-year treasury rate	0	✓	✓
EBP	Excess bond premium	0	✓	✓
NFCI	National financial conditions index	0	✓	
EXUSUKx	US/UK foreign exchange rate	0	✓	✓
OILPRICEx	Real crude oil prices (WTI)	2	✓	✓
SP500	S&P 500	2	✓	✓
EARGDP	Real gross domestic product (EA)	0		✓
JPRGDP	Real gross domestic product (JP)	0		✓
UKRGDP	Real gross domestic product (UK)	0		✓
USDEUR	EU/US foreign exchange rate	0		✓
JPUSD	JP/US foreign exchange rate	0		✓

B. ADDITIONAL EMPIRICAL RESULTS

(a) BART-het



(b) BVAR-het

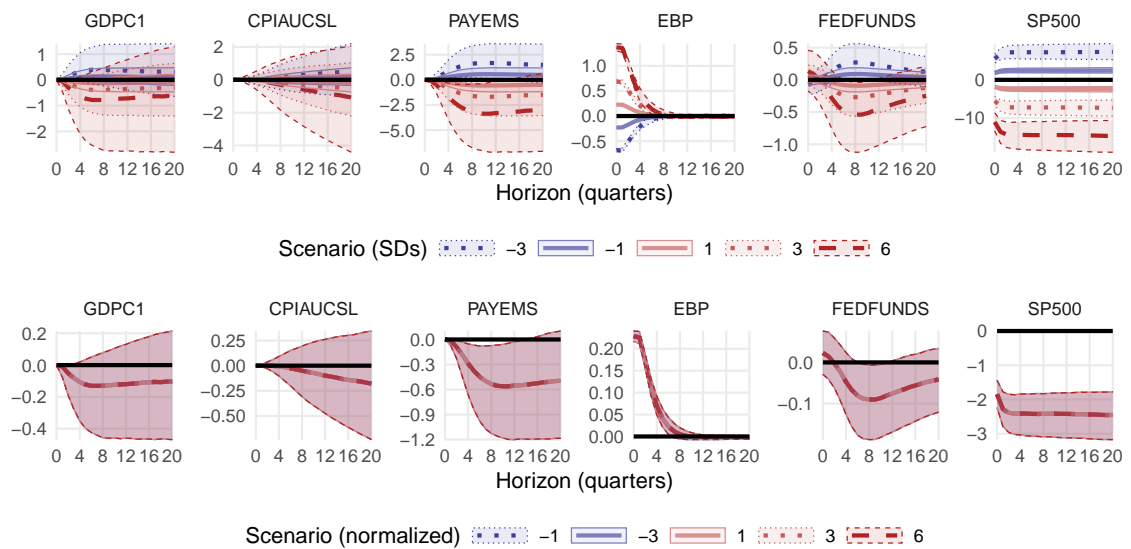


Figure B.1: Comparison of impulse response functions across nonlinear and linear models. Posterior medians alongside 68 percent credible sets. Cumulated responses for variables in differences and levels for all other variables.